Int J Multiphase Flow Vol 12, No 4, pp 627–640, 1986
Printed in Great Britain

0301-9322/86 $3.00 + .00
Pergamon Journals/Elsevier

PARAMETRIC EFFECTS ON THE VOID FRACTION MEASUREMENT BY CAPACITANCE TRANSDUCERS

MOON-HYUN CHUN and CHANG-KYUNG SUNG
Department of Nuclear Engineering, Korea Advanced Institute of Science and Technology, Seoul, Korea

(*Received* 4 *April* 1984, *in revised form* 19 *September* 1985)

Abstract—The main purpose of this work is to study the effects of (1) geometry, size and materials of electrodes, (2) flow pattern, and (3) electrode position with respect to a dielectric boundary on the void fraction measurement by capacitance transducers. A set of theoretical relative capacitance formulas for a test section, which is equipped with a pair of strip-type electrodes and in which an annular or stratified flow is present, is derived based on the concept of capacitance in series and parallel. From the experimental results, relationships between the measured relative capacitance and void fraction are obtained for both annular and stratified flow systems under static condition. This result is compared with theoretical predictions. From this study it is found that (1) the strip-type electrodes are more sensitive than ring-type electrodes for both annular and stratified flows, (2) electrode size does not affect the relative capacitance versus $(1 - \alpha)$ curve, and (3) electrode position is important for stratified flows but it has no effect on annular flows.

1. INTRODUCTION

Measurements of various flow parameters are essential in two-phase flow systems, such as primary and secondary nuclear reactor coolant systems. The response of the volumetric concentration of the liquid and vapor phases due to perturbations in heat flux and inlet flow is of particular interest due to its influence on the neutron dynamics in nuclear reactors. A knowledge of the vapor volume is needed for the determination of mean fluid density and acceleration, for the establishment of two-phase flow frictional pressure drop correlations, and for the computation of reactivity in water-cooled reactors.

Most of the void measuring techniques which are based on the effects of nuclear reactions, such as gamma attenuation, X-ray attenuation, beta attenuation, neutron diffusion or the (γ, n) reaction are not applicable inside the reactor cores where intensive fields of all these nuclear radiations predominate. Among the nonnuclear methods of void measurement, one of the most important is the capacitance method, which is based on the difference between liquid and vapor dielectric constants. This measuring method has been applied to determine the void fraction in bulk boiling by Cimorelli & Evangelisti (1978), to measure liquid film thickness by Leskovar *et al.* (1979) as well as to determine the particle velocity in gas–powder streams by Irons & Chang (1983).

While the basic methodology of this technique has been investigated to some extent by these previous workers, the experimental data on the effects and sensitivities of various parameters of the capacitance technique, such as geometry, size, material of electrode, flow pattern, and electrode position with respect to a dielectric boundary are not available in the open literature. The main purpose of this work is to examine the effects of (1) geometry, size, and materials of electrodes, (2) flow patterns, and (3) electrode position with respect to a dielectric boundary on the measurement of void fraction by the capacitance technique.

2. THEORY AND ANALYSIS

The void fraction measurement technique is based upon the facts that the dielectric constant of liquid water is a well defined parameter which is mainly a function of temperature; the value of the dielectric constant of the liquid or solid is very large compared to that of the gaseous phase. Depending on the flow pattern and size of bubbles, the total dielectric constant of a two-phase mixture can be calculated as a function of the dielectric constants of the two media by means of theoretical relations.

In order to compare with experimental results, a set of theoretical relative capacitance (C^*) formulas for a test section, which is equipped with a pair of strip-type electrodes and in which an annular or stratified flow is present are first derived by means of a simplified geometrical mapping and using the concept of capacitance in series and parallel.

In the derivation of analytical formulas, the following assumptions are made.

(1) No electrical fluxes are present on the exterior surface of the electrodes and at both ends of the electrodes where electrical insulation is made
(2) Two phases (i.e. liquid and vapor or liquid and solid) do not mix.

2.1 Relative capacitance formulas for core and annular flows

An isometric view and a cross section of the physical model with a pair of strip-type electrodes for an annular flow are shown in figures 1(a) and 2(a), respectively.

An equivalent void fraction α, which is the main variable of interest in this work, is first defined here as the ratio of areas (or volumes) of the coaxial dielectric cylinders of permittivities, ϵ_1 and ϵ_2 shown in figure 2(a):

$$\alpha = \frac{A_L}{A} = \frac{\pi d^2/4}{\pi D^2/4} = \left(\frac{d}{D}\right)^2 \qquad [1]$$

An equivalent cross section of figure 2(a), obtained by a graphical mapping using flux lines and equipotentials, is shown in figure 2(b). The capacitor system of figure 2(b) can be considered as combinations of capacitance in series and parallel, as illustrated in figure 2(c)

Using [1], functional relationships between the dimensions shown in figures 2(a) and 2(b) can be expressed as.

$$\begin{aligned} a &= \frac{\pi D}{2} \quad ; b = D \quad ; \\ h &= \frac{\pi d}{2} = \frac{\pi D\sqrt{\alpha}}{2} \quad , \\ d &= e = D\sqrt{\alpha} \quad ; \\ f &= \frac{b-e}{2} = \frac{D}{2}(1-\sqrt{\alpha}) \quad ; \\ g &= \frac{a-h}{2} = \frac{\pi D}{4}(1-\sqrt{\alpha}) \quad . \end{aligned} \qquad [2]$$

Total capacitance C of the system shown in figure 2(c) is given by:

$$C = \frac{1}{\frac{1}{c_1} + \frac{1}{c_{21} + c_{22} + c_{23}} + \frac{1}{c_3}} \qquad [3a]$$

$$= \frac{l\pi\epsilon_2[\epsilon_2(1-\sqrt{\alpha}) + \epsilon_1\sqrt{\alpha}]}{2[(\epsilon_1 - \epsilon_2)(\sqrt{\alpha} - \alpha) + \epsilon_2]} \qquad [3b]$$

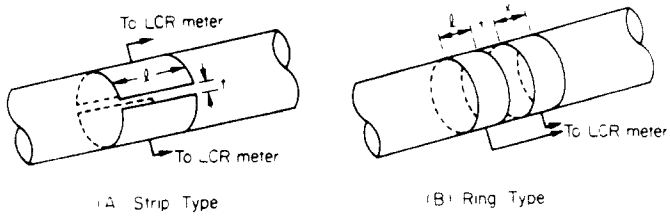

Figure 1 Isometric views of two different electrode configurations

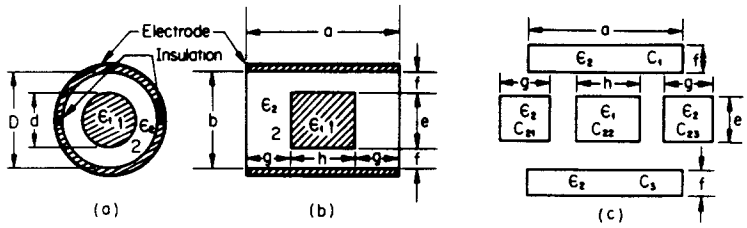

Figure 2 Cross section of a test section with a pair of strip-type electrodes for an annular flow (or a core flow).

Equation [3b] is derived from the following relations:

$$c_1 = c_3 = \frac{\epsilon_2 a l}{f} \quad ;$$

$$c_{21} = c_{23} = \frac{\epsilon_2 g l}{e} \quad ; \qquad [4]$$

$$c_{22} = \frac{\epsilon_1 h l}{e} \quad .$$

In order to eliminate the capacitances of the connecting cables and the pyrex tube, the relative capacitance C^* is defined as:

$$C^* = \frac{C - C_0}{C_1 - C_0} \text{ (when } \epsilon_1 > \epsilon_2) \qquad [5a]$$

$$C^* = \frac{C - C_1}{C_0 - C_1} \text{ (when } \epsilon_1 < \epsilon_2) \qquad [5b]$$

where

$$C_0 = [C]_{\alpha=0} = \frac{\pi \epsilon_2 l}{2} \qquad [6]$$

$$C_1 = [C]_{\alpha=1} = \frac{\pi \epsilon_1 l}{2} \qquad [7]$$

In the above equations, ϵ_1 is the permittivity of material 1, ϵ_2 the permittivity of material 2, l the length of electrode in axial direction, C_1 capacitance of the tube completely filled with liquid or solid (i.e. when $\alpha = 1$) and C_0 the capacitance of the empty tube (i.e. when $\alpha = 0$).

Equations [6] and [7] follow from [3b].

Substituting [3b], [6] and [7] into [5a] and [5b] the following equations are obtained:

$$C^* = \frac{\epsilon_2 \alpha}{(\epsilon_1 - \epsilon_2)(\sqrt{\alpha} - \alpha) + \epsilon_2}$$

$$= \frac{\epsilon_G (1 - \alpha)}{(\epsilon_L - \epsilon_G)(\sqrt{1 - \alpha} - 1 + \alpha) + \epsilon_G} \qquad [8a]$$

(for core flow and when $\epsilon_1 > \epsilon_2$)

$$C^* = 1 - \frac{\epsilon_2 \alpha}{(\epsilon_1 - \epsilon_2)(\sqrt{\alpha} - \alpha) + \epsilon_2}$$

$$= 1 - \frac{\epsilon_L \alpha}{(\epsilon_G - \epsilon_L)(\sqrt{\alpha} - \alpha) + \epsilon_G} \qquad [8b]$$

(for annular flow and when $\epsilon_1 < \epsilon_2$)

where ϵ_L is the permittivity of the liquid phase and ϵ_G the permittivity of the vapor phase Equations [8] can also be expressed in terms of dielectric constant ϵ_R (or relative permittivity) which is defined by $\epsilon_R = \epsilon/\epsilon_0$:

$$C^* = \frac{\epsilon_{2R}(1 - \alpha)}{(\epsilon_{1R} \quad \epsilon_{2R})(\sqrt{1 - \alpha} \quad 1 + \alpha) + \epsilon_{2R}} \qquad \text{(for core flow and when } \epsilon_1 > \epsilon_2) \quad [9a]$$

$$C^* = 1 - \frac{\epsilon_{2R}\alpha}{(\epsilon_{1R} - \epsilon_{2R})(\sqrt{\alpha} \quad \alpha) + \epsilon_{2R}} \qquad \text{(for annular flow and when } \epsilon_1 < \epsilon_2) \quad [9b]$$

It may be noted here that in the transformation from the equivalent void fraction α defined by [1] to the actual void fraction α in [8] the following intermediate steps between figures 2(a) and 2(b) are used along with a few simplifying approximations: a curvilinear square field mapping method described by Hippel (1954) is first employed to divide the field containing region of figure 2(a) into curvilinear squares by the equipotential surfaces between two electrodes and electric flux lines. Each curvilinear square differs from a true square in having slightly curved and slightly unequal sides but approaches a square as its dimensions decrease. This method is applicable only to fields in which no variation exists in the direction normal to the surface of the paper. The curvilinear-square field is then mapped on the two parallel electrodes as represented by figure 2(b). The main approximations introduced in this step are:

(1) For the case of annular flow, the equivalent void fraction α is defined based on a cylindrical geometry as given by [1], whereas the capacitive contributions of the liquid and vapor regions are calculated on the basis of layers of materials between infinite flat plates as shown in figure 2(b) and a uniform electric field.
(2) The spacing between the strip-type electrodes is assumed to be equivalent to the diameter of the pipe. This assumption may appear to be the main source of error in the analytical expressions given by [8] or [9] since the largest contributions to the measurement occur near the insulation between the two electrodes. Therefore, a qualitative examination of [9] is made to examine the validity of the above approximations

2.2 Relative capacitance formulas for stratified flows

For stratified flows, there are two typical configurations depending on the position of strip-type electrodes with respect to the dielectric boundary as shown in figure 3. The following two terms are defined for convenience in discussion:

Horizontal Electrode Position—This is the case when the dielectric boundary (i.e. the interface between the two different materials with permittivities of ϵ_1 and ϵ_2) is parallel to the imaginary line connecting two insulation points between a pair of strip electrodes attached circumferentially on the surface of a test section (figure 3a).

Vertical Electrode Position—The configuration of strip electrodes is such that the dielectric boundary is vertical to the imaginary line joining two insulation points between a pair of electrodes (figure 3b)

(1) For Horizontal Electrode Position (figure 3a): In a manner similar to the derivation of [9] the following equations are obtained as shown in the Appendix:

$$C^* = \frac{\epsilon_{2R}\,\theta(1 - \cos\theta)}{\epsilon_{2R}\,\pi - (\epsilon_{2R} - \epsilon_{1R})\theta(1 + \cos\theta)} \qquad \left(\text{If } \epsilon_{1R} > \epsilon_{2R} \text{ and } 0 \le \theta \le \frac{\pi}{2}\right) \quad [10a]$$

$$C^* = \frac{\epsilon_{1R}\pi + (\pi - \theta)[\epsilon_{2R}(1 - \cos\theta) - 2\epsilon_{1R}]}{\epsilon_{1R}\pi + (\epsilon_{2R} - \epsilon_{1R})(\pi - \theta)(1 - \cos\theta)} \qquad \left(\text{If } \epsilon_{1R} > \epsilon_{2R} \text{ and } \frac{\pi}{2} \le \theta \le \pi\right) \quad [10b]$$

where ϵ_{1R} is the dielectric constant of the material 1 and ϵ_{2R} the dielectric constant of material 2.

Similar expressions can be obtained for $\epsilon_{2R} > \epsilon_{1R}$ and $0 \le \theta \le \pi/2$, and for $\epsilon_{2R} > \epsilon_{1R}$ and $\pi/2 \le \theta \le \pi$. In [10], θ is the stratified angle shown in figure 3

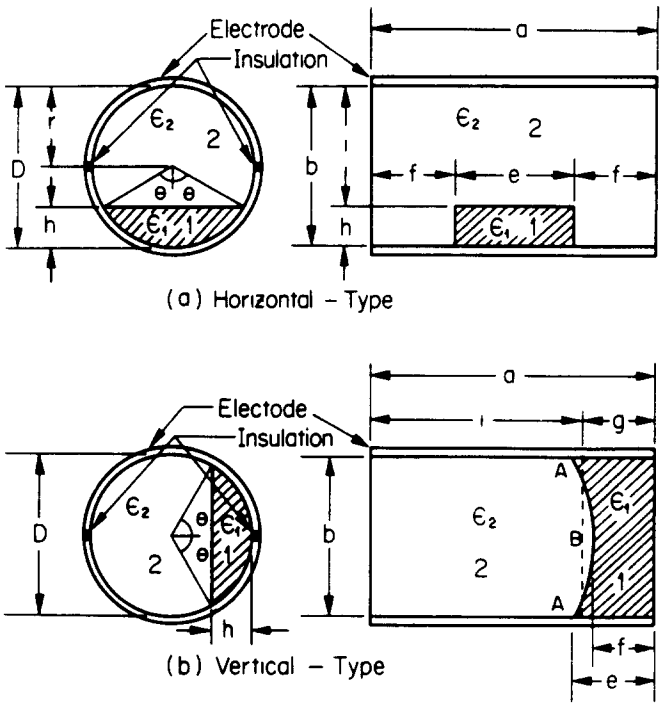

Figure 3. Cross sections of two test sections with a pair of strip-type electrodes for stratified flows.

(2) For Vertical Electrode Position (figure 3b): Following the same procedure used in the derivations of [9] and [10], the following simple equations are obtained:

$$C^* = \frac{\pi(1 - \cos\theta) + 2\theta}{4\pi} \qquad (\text{If } \epsilon_1 > \epsilon_2) \qquad [11a]$$

$$C^* = \frac{\pi(3 + \cos\theta) - 2\theta}{4\pi} \qquad (\text{If } \epsilon_1 < \epsilon_2) \qquad [11b]$$

In the derivation of [11], the interface between the materials ϵ_1 and ϵ_2 is approximated by a dotted straight line as shown in figure 3(b). In [11] C^* is independent of $\epsilon_R's$ and depends only on α (since θ is determined solely by α).

2.3 Comparison of [9] with Maxwell formulas

Before making a comparison between experimental results and theoretical predictions, a qualitative examination of [9] is made here. Approximate formulas relating α to the relative capacitance (C/C_1), according to the Maxwell law, are derived by Cimorelli *et al.* (1978) for two flow patterns: (1) one for small size bubbles dispersed in water matrix (whose flow pattern is similar to an annular flow, and (2) the other for small liquid masses dispersed in a vapor matrix (similar to a core flow).

In figure 4, predictions of [9] compared with the results of the Maxwell formulas. The values of ϵ_R for water and air used in [9] are 55 and 1, respectively as listed in table 2(b). Considering the difference in the flow patterns used in [9] and Maxwell formulas, the close agreement between the two predictions, as can be seen in figure 4, is rather surprising.

3. EXPERIMENTAL APPARATUS AND TEST METHOD

3.1 Apparatus description

The apparatus of the present stationary experiment consists of three major parts as shown in figures 5 and 6: (1) two types of test sections, one with a pair of strip-type electrodes (figure 1(a), the other with a pair of ring-type electrodes (figure 1(b), (2) simulation models for various void fraction and flow patterns (figure 6), and (3) measuring equipment.

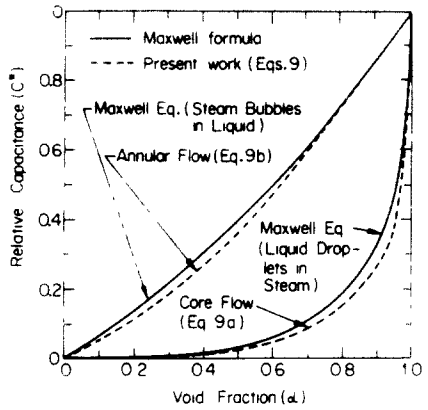

Figure 4 Comparison of theoretical curves of the present work with Maxwell formulas

The test section is a cylindrical pyrex tube where a pair of electrodes are attached circumferentially and then a simulation model is inserted. This was wrapped with a rubber sheet (1 mm thick) and then electrostatically shielded with an aluminium foil as can be seen in figure 5. Dimensions of test sections and electrodes are given in table 1

The void fraction and flow pattern, such as annular or stratified flow in static condition, were controlled and simulated by inserting a known amount of water or by inserting a different simulation model (shown in figure 6) with a known size into the test section. Dimensions and dielectric constants of flow pattern models are shown in table 2.

The capacitance was measured with a digital LCR meter (HP model 4262 A) that has the measuring range of capacitance from 0.01 pF to 19.99 mF.

3.2 Test parameters

The main controllable test parameters were: (1) flow pattern (annular and stratified), (2) electrode type (strip or ring) and its position on the test section with respect to the dielectric boundary (vertical or horizontal), (3) void fraction (from zero to unity) and (4) test section diameter. These test parameters can be further classified as shown in table 3.

As may be observed in [9] and [10] the relative capacitance is functions of dielectric constants ϵ_R, void fraction α (or stratified angle θ), except for the case of vertical type of stratified flows with a pair of strip-type electrodes. Void fractions and flow patterns were simulated with a proper combination of two different materials having different dielectric constants.

In the preliminary test, the sensitivity and flow regime dependency of two basic electrode types (i.e. ring- and strip-type) were first examined and evaluated along with the sensitivity of LCR meter frequency. As a result, LCR meter frequency of 10 kHz and the strip-type electrode were selected to be used in all the final series of tests.

3.3 Test procedures

For each test, the following procedure is required:

(1) The load cable from a pair of electrodes is first connected to the LCR meter as shown in figure 5

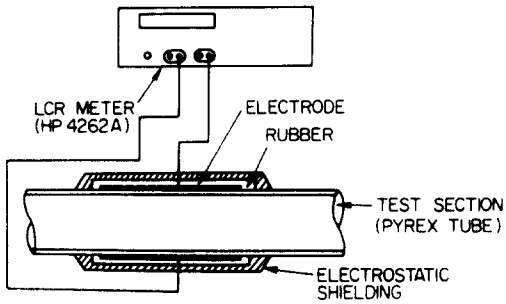

Figure 5 Schematic diagram of experimental apparatus

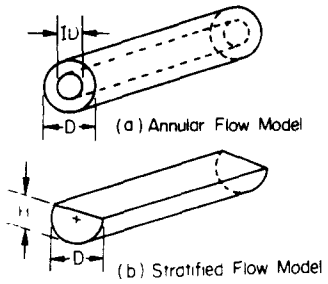

Figure 6. Isometric view of flow pattern model.

(2) The capacitance of the leads and the empty tube (i.e. C_0) is then measured along with the capacitance of the leads and the tube which is completely filled with void fraction or flow pattern simulant material (i.e. C_1).
(3) The output capacitance of the whole test section partially filled with a given void fraction or flow pattern model (i.e. C), which has a known dielectric constant and volume, is measured.
(4) An experimental value of the relative capacitance C^* is then obtained by substituting the above measured values of C, C_0, and C_1 into [5a] or [5b].

4 EXPERIMENTAL RESULTS AND COMPARISON WITH THEORY

From the experimental results, a relationship between the measured relative capacitance (C^*) of the strip and ring electrodes and void fraction (in the form of $1 - \alpha$), in annular and stratified flow systems under static condition, is obtained for various combinations of test parameters, and this result is compared with theoretical predictions. A brief summary of important results are as follows:

Table 1. Test section geometry and other data

(a) Test section dimensions

Material	I.D. (mm)	O.D. (mm)	Length (mm)	Volume (cc)	Test Section No.
Pyrex Tube	34.5	38.5	250	234	Tube-1
Pyrex Tube	26	30	250	133	Tube-2

(b) Electrode dimensions attached to each test section

Electrode Type	Material and Electrode No.	Width W (mm)	Length ℓ (mm)	Gap (t) (mm)	Attached Test Section	Flow Model Material
Strip	Al-1	46	40	4	Tube-2	polyacrylate ; water
	Al-2	46	50	4	"	polyacrylate
	Al-3	46	57	5.6	"	paraffin wax
	Al-4	46	60	3.5	"	polyacrylate
	Al-5	60	70	4	Tube-1	water
	Al-6	46	80	3.75	Tube-2	water
	Al-7	46	99	5.5	"	paraffin wax
	Cu-1	46	50	3.5	Tube-2	water ; polyacrylate
	Cu-2	46	60	4	"	water
	Cu-3	60	45	3.5	Tube-1	water
Ring	Al-R	94	10		Tube-2	polyacrylate

Table 2 Dimensions and dielectric constants of flow pattern models

Flow Pattern	Model No.	D(Fig.6) (mm)	ID(or H) (Fig.6) (mm)	Void Fraction	Flow Model Material
Annular	A-1	26	0	0	paraffin wax
	A-2	"	4.5	0.03	"
	A-3	"	8.04	0.14	"
	A-4	"	15.85	0.42	"
	A-5	"	18.9	0.51	"
	B-1	"	0	0	polyacrylate
	B-2	"	8.46	0.11	"
	B-3	"	11.68	0.20	"
	B-4	"	13.12	0.25	"
	B-5	"	16.20	0.39	"
	B-6	"	20.42	0.61	"
	B-7	"	23.02	0.79	"
Stratified	C-1	26	26	0	polyacrylate
	C-2	"	20.17	0.17	"
	C-3	"	18.11	0.26	"
	C-4	"	15.10	0.40	"
	C-5	"	13.45	0.48	"
	C-6	"	12.11	0.54	"

(b) Dielectric constants of flow pattern material given by Hippel (1954)

Material	Dielectric Constant ε_R	Temperature (°C)
Water	78.2	25
	55	102
Air	1	102
Paraffin wax	2.25	25
Polyacrylate	2.75	23

4.1 Flow regime dependence of C versus (1 − α) curve and sensitivities of ring and strip electrodes

The flow regime dependence of the "output capacitance $(C - C_0)$ versus $(1 - \alpha)$ curve" is shown in figure 7 for both ring and strip electrodes. From this figure one may observe that the strip electrodes are, in general, far more sensitive than ring electrodes for both annular and stratified flows.

Table 3. Classification of main test parameters

Test Parameters:	Flow Pattern	Electrode	Void Fraction	Test Section Size
(1) Types	a) Annular flow b) Stratified flow	a) Ring-type b) Strip-type	N/A	a) Tube-1 b) Tube-2
(2) Material or combination of simualtion material :	a) Paraffin wax and air b) Polyacrylate and air c) Water and air	a) Aluminium b) Copper	a) Paraffin Wax and air b) Polyacrylate and air c) Water and air	Pyrex Tube
(3) Size or Range of measurement :	N/A	Listed in Table 1(b)	α =0∿1 Listed in Table 2	Listed in Table 1(a)
(4) Position of electrode with respect to dielectric boundary	N/A	a) Horizontal b) Vertical c) 80 degree	N/A	N/A

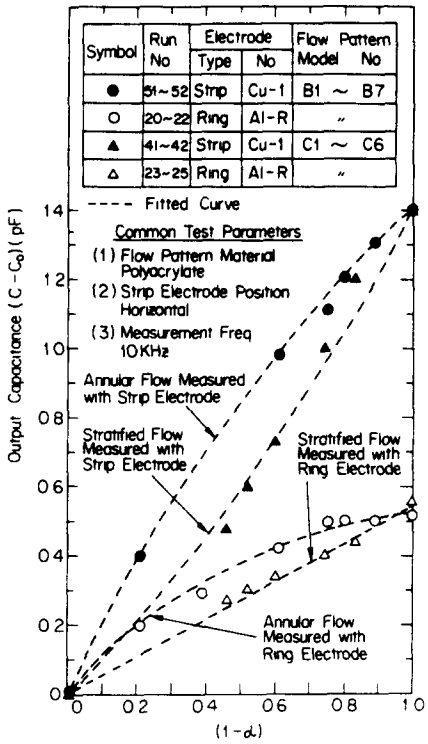

Figure 7 Flow regime dependence of $(C - C_0)$ versus $(1 - \alpha)$ curve and sensitivities of ring and strip electrodes

Therefore, the strip-type electrodes are employed in all of the tests of other parameters in this work.

4.2 Effect of the electrode size and flow pattern material on C versus (1 − α) curve*

Figure 8 shows that C^* versus $(1 - \alpha)$ curve depends on the flow pattern material, but does not depend on the electrode size, whereas the output capacitance $(C - C_0)$ increases with increase in electrode size. The sensitivity of C can be improved by using larger electrodes.

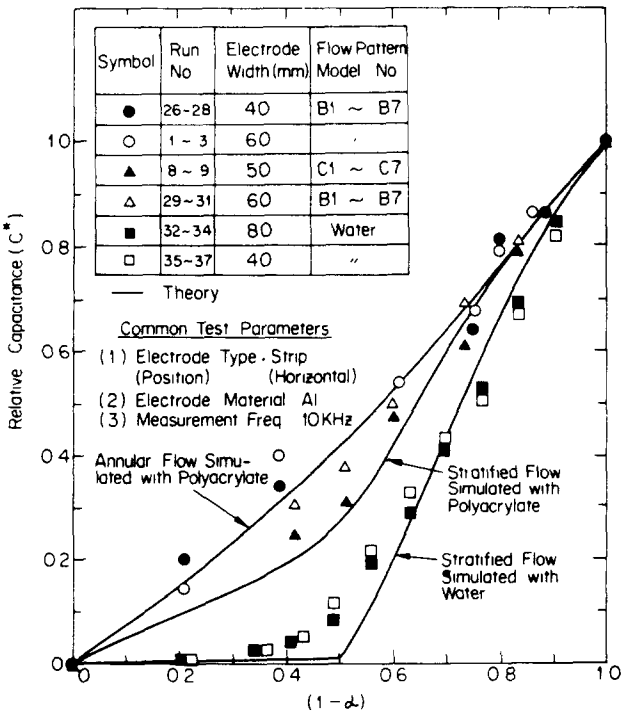

Figure 8 Effect of electrode size and flow pattern material on C^* versus $(1 - \alpha)$ curve

4.3 Effect of electrode configuration on C^* versus $(1 - \alpha)$ curve

Reproducibility and the effect of strip-type electrodes position on the C^* versus $(1 - \alpha)$ curve for annular and stratified flows are shown in figures 9 and 10, respectively While figure 9 indicates that the C^* versus $(1 - \alpha)$ curve does not depend on electrode position for annular flow, figure 10 shows that it depends on the electrode position for stratified flow

4.4 Effect of electrode material on C^* versus $(1 - \alpha)$ curve

Two materials for strip electrodes (i.e. Al and Cu) are tested to evaluate the sensitivity and possible effects of electrode material on the measurement of C^* versus $(1 - \alpha)$. However, no visible effect can be observed from the experimental results shown in figure 11.

4.5 Accuracy of the results

To evaluate approximately the accuracy of the results obtained with the capacitance method, measured values of $(1 - \alpha)$ are compared with true values of $(1 - \alpha)$ as shown in figure 12. The measured values of $(1 - \alpha)$ in figure 12 are obtained by substituting the relative capacitance measured by a capacitance transducer into the theoretical formulas derived in the present work such as in [9b], [10], or [11]. True values of $(1 - \alpha)$, on the other hand, correspond to those values simulated by inserting a different simulation model with known size (listed in table 2) into the test section (or controlled inserting a known amount of water into the test section).

As can be seen in figure 12, the agreement between the measured values and true values is within $\pm 10\%$ with some exceptions of the results that were obtained for stratified flow simulated with water at lower $(1 - \alpha)$ values than 0.5. In figure 8, it must be noticed that when stratified flow is simulated by water (and air), in particular, the slope of the C^* versus $(1 - \alpha)$ curve is extremely small until $(1 - \alpha)$ value reaches 0.5; the main reason for this is because there is a large difference in dielectric constants of water (55 at 102°C) and air (1 at 102°) as shown in table 2(b). Consequently, small fluctuations in measurements due to finite precision of instruments used in making the capacitance measurements can introduce large relative errors in the region of small $(1 - \alpha)$ values.

Instrumental errors of the present work are mainly associated with the accuracy of the LCR meter (HP model 4262 A); the accuracy of the LCR meter is 3% of the reading plus counts according to its specifications.

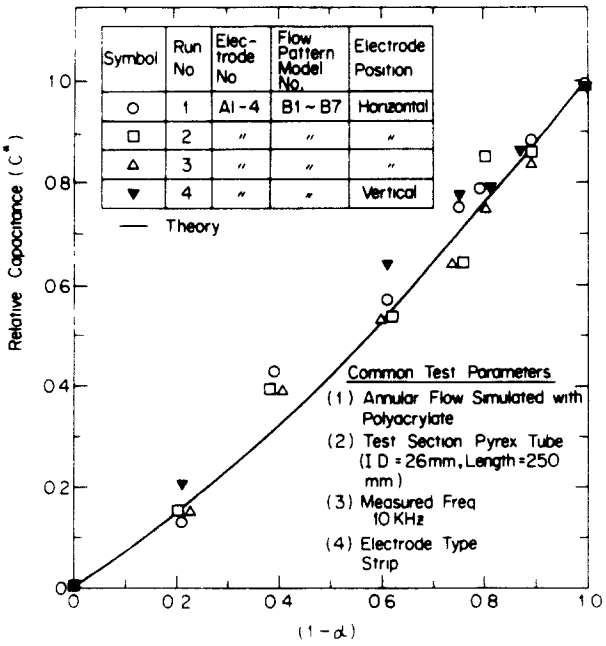

Figure 9 Reproducibility and effects of electrode configuration on C^* versus $(1 - \alpha)$ curve for annular flow.

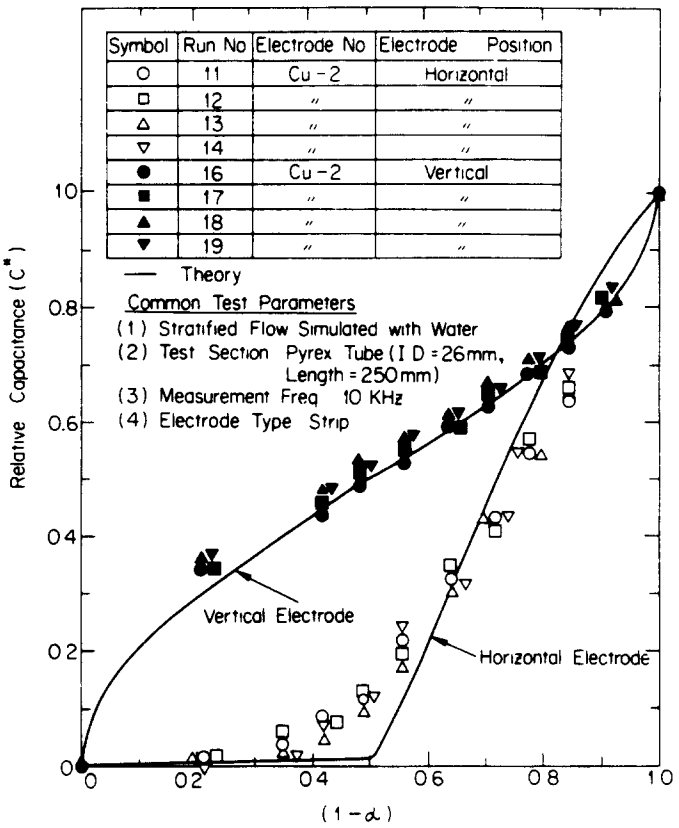

Figure 10. Reproducibility and effects of electrode configuration on C^* versus $(1 - \alpha)$ curve for stratified flow.

5. CONCLUSIONS

From the present theoretical analysis and experimental results the following conclusions can be made:

(1) Strip-type electrodes are more sensitive than ring electrodes for both annular and stratified flows.

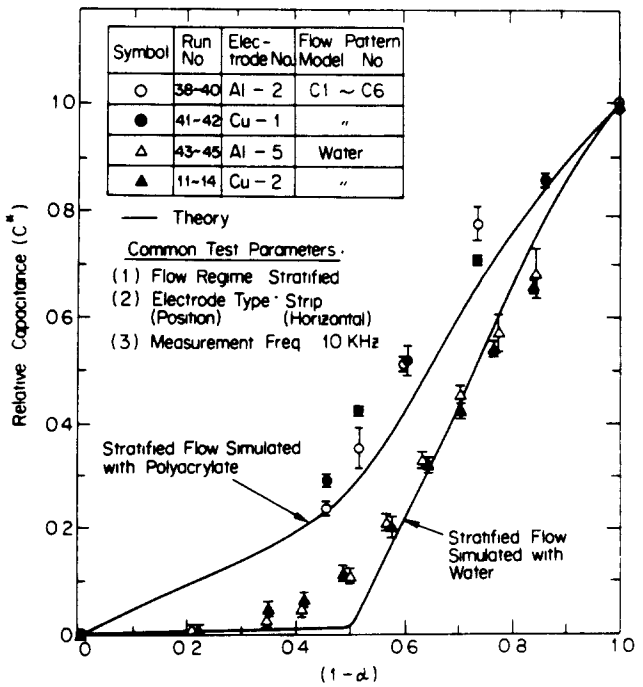

Figure 11. Effects of electrode material on C^* versus $(1 - \alpha)$ curve.

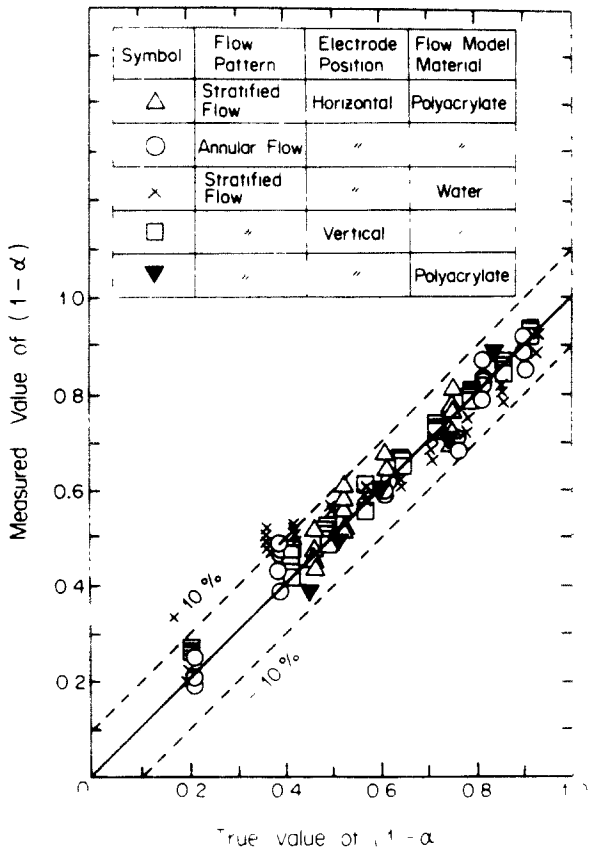

Figure 12 Comparison of experimental and true $(1 - \alpha)$ value

(2) The electrode length, within the values tested, had no effect on the relative capacitance versus $(1 - \alpha)$ curve, but the sensitivity of the output capacitance (C) can be improved by increasing the electrode size.
(3) Electrode position is important for stratified flows, but it has no effect for annular flows. Since the vertical electrode position gives larger values of C^* than the horizontal electrode position, the vertical electrode position should be used for stratified flows in particular.
(4) In general, the agreement between the predicted values of $(1 - \alpha)$ and the experimental results is within $\pm 10\%$.
(5) Without independent knowledge of the flow pattern the void fraction cannot be determined. Therefore, it is necessary to determine the flow pattern of the given two-phase flow system before making the void fraction measurement by means of the capacitance transducer technique.

Acknowledgements—This work was supported by the Korea Science and Engineering Foundation.

REFERENCES

CIMORELLI, L. & EVANGELISTI, R. 1978 The application of the capacitance method for void fraction measurement in bulk boiling conditions. *Int. J. Heat Mass Transfer* **10**, 277–288.

HEWITT, G. F. 1982 Measurement of void fraction. *Handbook of Multiphase System* (Edited by G. Hetsroni), pp. 10.21–10.33. Hemisphere/McGraw-Hill, New York.

HIPPEL, A. R. V. 1954 *Dielectric Materials and Applications*, pp. 335–361, MIT Press, MIT, Cambridge, Mass.

IRONS, G. A. & CHANG, J. S. 1983 Measurement of void fraction and particle velocity in gas–powder streams by capacitance transducers. A draft paper obtained via a personal communication.

KAYT, W. H. Jr. 1982 *Engineering Electromagnetics*, 4th Edn., pp. 177–183, McGraw-Hill, New York.

LESKOVAR, B., SUN, R. K., KOLBE, W. F. & TURKO, B. 1979 Measurement of the thickness of liquid film by means of capacitance method. Electric Power Research Institute Report, NP-1212, Palo Alto, California.

APPENDIX

Derivation of the relative capacitance formula for stratified flows [10a]:

The left-hand side of figure 3(a) is the horizontal-type test section with a pair of strip-type electrodes for stratified flow, whereas the right-hand side of figure 3(a) shows the equivalent cross section obtained by the curvilinear square field mapping method described by Hippel (1954) on an equivalent parallel-plate capacitor containing two dielectrics with the dielectric interface parallel to the conducting plates ("*e*" in figure 3a).

As in the case of the annular flows, an equivalent void fraction α is defined as

$$\alpha = \frac{A_1}{A} = \frac{2\theta - \sin 2\theta}{2\pi} \qquad [A.1]$$

Dimensions shown on the right-hand side of figure 3(a) can be expressed in terms of the inside diameter of the test section D and the stratified angle θ as follows:

$$\begin{aligned} a &= \frac{\pi D}{2} \quad ; b = D \quad ; \\ e &= \frac{D}{2}(2\theta) = D \quad ; \\ f &= \frac{(a - e)}{2} = \frac{D}{2}\left(\frac{\pi}{2} - \theta\right) \quad ; \\ h &= \frac{D}{2} - \frac{D}{2}\cos\theta = \frac{D}{2}(1 - \cos\theta) \\ i &= b - h = \frac{D}{2}(1 + \cos\theta) \end{aligned} \qquad [A.2]$$

In a manner similar to the figures shown in figure 2(c), the total capacitance C of the system shown on the right-hand side of figure 3(a) can be considered as a combination of four smaller capacitors. That is,

$$C = \frac{1}{\dfrac{1}{C_1} + \dfrac{1}{C_{21} + C_{22} + C_{23}}} \qquad [A.3]$$

where

$$\begin{aligned} C_1 &= \frac{\epsilon_2 a l}{i} \quad ; \\ C_{21} &= \frac{\epsilon_2 f l}{h} \quad ; \\ C_{22} &= \frac{\epsilon_1 e l}{\mathrm{h}} \quad ; \\ C_{23} &= \frac{\epsilon_2 f l}{h} \end{aligned} \qquad [A.4]$$

First, substituting [A.2] into [A.4] and using the results in [A.3] the following expression can be obtained:

$$C = \frac{l\epsilon_2\pi\,[\epsilon_2\pi - (\epsilon_2 - \epsilon_1)2\theta]}{2\epsilon_2\pi - 2(\epsilon_2 - \epsilon_1)\theta(1 + \cos\theta)} \qquad [A.5]$$

Finally, substituting [A.5], [6] and [7] into [5a]

$$C^* = \frac{\epsilon_2\theta(1 - \cos\theta)}{\epsilon_2\pi - (\epsilon_2 - \epsilon_1)\theta(1 + \cos\theta)} \qquad [A.6]$$

When [A.6] is expressed in terms of dielectric constants the following equation is obtained:

$$C^* = \frac{\epsilon_{2R}\theta(1 - \cos\theta)}{\epsilon_{2R}\pi - (\epsilon_{2R} - \epsilon_{1R})\theta(1 + \cos\theta)} \qquad [A.7]$$

Equation [A.7] is the same as [10a], and this equation is applicable for $0 \leqq \theta \leqq \pi/2$ if $\epsilon_{1R} > \epsilon_{2R}$. Following the same procedure as in the derivation of [10a] the remaining equations [10b], [11a], and [11b] can be derived.